This article has been accepted for publication in a future issue of this journal, but has not been fully edited. Content may change prior to final publication. Citation information: DOI 10.1109/TIE.2018.2795519, IEEE Transactions on Industrial Electronics

Submodule Voltage Estimation Scheme in Modular Multilevel Converters with Reduced Voltage Sensors Based on Kalman Filter Approach

[1]Osama SH. Mohamed Abushafa, Mohamed S. A. Dahidah, *Senior Member, IEEE*, Shady M. Gadoue and David J. Atkinson, *Member, IEEE.*

***Abstract*— This paper presents a new voltage estimation method for the submodule (SM) capacitor in a modular multilevel converter (MMC). The proposed method employs a Kalman filter (KF) algorithm to estimate the SM voltages of the converter. Compared with sensor-based methods, this scheme requires only one voltage sensor to achieve the voltage-balancing of the converter. This sensor is connected to the total arm voltage; the proposed algorithm requires also the switching patterns of each upper SM switch which are provided by the controller used without the need for extra sensors. The substantial reduction in the number of voltage sensors improves the system reliability and decreases its cost and complexity. Extensive simulation and experimental analyses carried out to validate the proposed estimation scheme under different conditions include steady-state analyses, the effect of variations in capacitance and inductance, of the impact of low carrier and effective switching frequency on the accuracy of the estimation, step changes to the load, and a range changes in DC voltage. The results obtained are experimentally verified using a single-phase MMC.**

***Index Terms*— Modular multilevel converter (MMC); capacitor voltage estimation; Kalman filter (KF); reduced number of sensors; voltage-balancing control; pulse width modulation (PWM).**

I. INTRODUCTION

Since the modular multilevel converter (MMC) was introduced in 2003 [1] it has become a competitive candidate for many medium and high power applications. In comparison with conventional multilevel converters, MMCs are characterized by low switching losses due to the low switching operating frequency required, flexibility [2], and low harmonic distortion which allows the use of smaller filters. MMCs have been proven to be suitable for different applications such as electrical vehicles, variable speed drives, high-voltage direct current systems (HVDC), battery storage systems (BSSs), DC-DC power conversion and flexible AC transmission systems (FACTSs) [3, 4].

On the other hand, as with most conventional converters, the MMC has specific control requirements. For instance, the voltage-balancing of the submodule (SM) capacitors in the converter is critical. However, due to the series of cascaded SMs which are used to construct the converter, the reliability of the MMC is an important challenge [5]. In one example of a real application based on the MMC is presented in [6], where hundreds of SMs per leg were used. This also requires a great many voltage sensors in order to achieve the voltage-balancing of the system. This problem has been extensively investigated in recent research [3, 7]; but many voltage sensors are always used in such studies. However, it would be preferable if this issue could be resolved with lower cost and complexity.

Several proposals have been attempted to minimise the number of voltage and current sensors required. For instance, successful simulation and practical results have been achieved with fewer current sensors [8-10]. However, no reductions in voltage sensor number were discussed in those studies. Another attempt based on an open-loop scheme has been suggested, where fixed PWM signals were applied to the converter [11]. Although, this proposed scheme does not use any sensors since it does not require any form of feedback control, the well-known disadvantages of open-loop control schemes may threaten the performance of the system. In some recent studies, online observers have been introduced to estimate individual SM voltages [12, 13]. For example, fewer voltage sensors could be achieved based on a sliding mode where the proposed method merely monitors the total input voltage and arm current of the converter [12]. This technique has been proposed for fault detection scheme. However, variations in SM capacitance were not considered in this study. In an attempt to ameliorate this problem, the estimation of capacitance values for each individual SM was considered in [13]. This improvement provides an important solution against concerning capacitance; however, in all observer-based methods the effect of variations associated with arm inductor values was not included in the design. In very recent research [14, 15], the voltage-balancing of a seven-level MMC has been achieved with important reductions in the number of voltage sensors required, where the lowest number of voltage sensors needed is two when seven-level MMC is used. Two sensors are contributed to measure total arm voltage of the converter. On the other hand, the main

Manuscript received January 27, 2017; revised June 04, 2017 and October 20, 2017; accepted December 27, 2017. This work was supported by Libyan Ministry of Higher Education and Scientific Research and Scholar Program of Zawia and Sabratha Universities.
Osama SH. Mohamed Abushafa is with Turbo Power Systems LTD company and also with the Department of Electrical Engineering, Faculty of Engineering, Sabratha University, Libya (e-mail: oabushafa@turbopowersystems.com).
Mohamed S. A. Dahidah and Dave G. Atkinson are with the School of Engineering, Newcastle University, Newcastle upon Tyne, NE1 7RU, UK (email: mohamed.dahidah@ncl.ac.uk; dave.atkinson@ncl.ac.uk.)
S. M. Gadoue is with the School of Engineering and Applied Science, Aston University, Birmingham, B4 7ET, U.K., and also with the Department of Electrical Engineering, Faculty of Engineering, Alexandria University, Alexandria 21544, Egypt (e-mail: s.gadoue@aston.ac.uk).

This article has been accepted for publication in a future issue of this journal, but has not been fully edited. Content may change prior to final publication. Citation information: DOI 10.1109/TIE.2018.2795519, IEEE Transactions on Industrial Electronics

concern with this method is that an advanced voltage-balancing method must be incorporated to guarantee stability.

This paper proposes a new voltage estimation scheme which aims to reduce the number of voltage sensors required in the MMC. The arrangement of sensors used is similar to those presented in previous studies [14, 15]. However, the proposed scheme uses only one voltage sensor per arm to achieve the voltage-balancing of the converter. Each sensor is connected to the total arm output voltage of the SMs. For the first time in MMC applications, and for the purpose of estimating the voltage across each SM capacitor, the proposed method here applies a Kalman filter (KF) algorithm. In comparison to some recursive algorithms, KF is more capable of reducing the side effects caused by sensor noise. A most valuable contribution of the proposed technique is that only the measured total arm voltage and the switching states of the SMs are required. The values of the switching states are accessed directly from the digital signal processor (DSP) controller, which means that no extra sensors are required. Unlike in some previously proposed schemes, the proposed scheme does not require an advanced voltage-balancing method. Extensive evaluations have been conducted into the effect of variations in SM capacitance on the algorithm's performance. Further steady-state and dynamic analyses are detailed in the main part of the paper. This contains: the effect of low carrier frequency on the estimation results, up and down step changes in load conditions, and extreme range changes in DC voltage. In addition to its potential to decrease cost and complexity, the proposed method might also be used for fault detection algorithms with the aim of improving the general performance of the MMC.

II. MMC Structure

One leg (single-phase) of the MMC is considered in this research, although the proposed estimation scheme can simply be applied to three-phase MMCs. The circuit configuration of the one-leg MMC is illustrated in Fig.1. This leg consists of upper and lower arms, each of which comprises of a number of cascaded SMs which are connected in series with an arm inductor (L_s). Only the half-bridge configuration is presented in Fig. 1(b), however, other arrangements have been combined with the MMC in recent studies. For example, the three-level neutral point clamped (NPC), full-bridge and three-level flying capacitor (FC) can be used in the SM instead of the half-bridge [16]. Each of these arrangements has its own features, and the application used with the MMC will determine which is more suitable for the system in terms of the efficiency level required [17].

Table I shows the relationship between the SM switches and the SM state for the half-bridge arrangement. The states of the SM are decided by two switches, S_x and $\overline{S_x}$. For instance, when S_x is switched **ON**, the SM (V_{SM}) voltage will be equal to the capacitor (C_x) voltage (V_{cx}), where $x = 1,2, \ldots 2n$, and n is the number of SMs per arm. Note that the voltage drop caused by S_x is neglected. Nevertheless, $\overline{S_x}$ must be **OFF**, and this is known as an **ON** state. In contrast; when the switch $\overline{S_x}$ is **ON** and the switch S_x is **OFF** the output of the SM is bypassed i.e. it is equal to zero [18].

The upper (i_u), lower (i_l) and circulating (i_{cir}) current in relation with the load current (i_{load}) are defined as follows [19]:

$$i_u = i_{cir} + \frac{i_{load}}{2} \quad (1)$$

$$i_l = i_{cir} - \frac{i_{load}}{2} \quad (2)$$

Meanwhile the output voltage of the MMC (u_a) is given by [9]:

$$u_a = \frac{u_l - u_u}{2} - \frac{L_s}{2}\frac{di_{load}}{dt} \quad (3)$$

In equation (3), u_u is the total voltage between the first SM and n SM while u_l is the total output voltage of the lower SMs (from $(n+1)$ to $2n$) as described in Fig. 1(a).

TABLE I
SM STATES

State of the SM	S_x	$\overline{S_x}$	V_{SM}
ON	**ON**	**OFF**	V_{cx}
Bypassed	**OFF**	**ON**	0

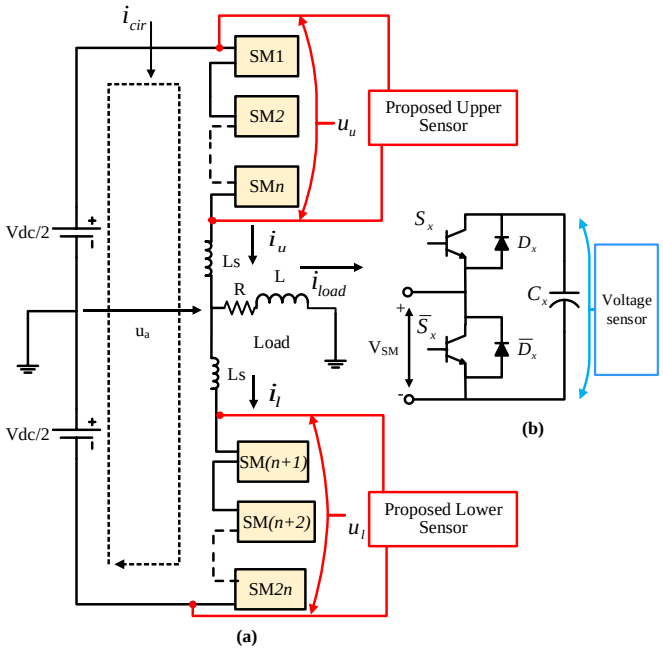

Fig. 1. Single-phase MMC structure. (a) The proposed sensor arrangement for one-leg. (b) Half-bridge SM arrangement with sensor-based SM arrangement.

III. Proposed Estimation Scheme for MMCs

A. MMC Voltage Modelling and Sensor Arrangement

The proposed method is applied to a single-phase MMC based on the half-bridge configuration as described earlier in Fig.1. Only two voltage sensors are required to achieve the voltage-balancing of one leg of the converter. The proposed sensors arrangement is illustrated in Fig. 1(a), where the upper sensor is connected between the top cell of the arm to the bottom cell terminals within the same arm, whilst the second sensor is positioned between. $SM_{(n+1)}$ and SM_{2n}.

In this research, only the MMC with the half-bridge configuration is examined. However, the proposed estimation

method can also be applied to other multilevel converters, such as the cascaded H-bridge converter (CHC) and flying capacitor converter (FCC). The only difference required is to consider the specific relationship between the state of the capacitor and its related switches.

The relationship between the output upper and lower arm voltages, individual SM voltages and semiconductor switching states for an *N*-level MMC can be derived as follows:

$$\begin{aligned} u_u(t_0) &= S_1(t_0)\,V_{c1}(t_0) + \cdots + S_n(t_0)\,V_{cn}(t_0) \\ u_u(t_1) &= S_1(t_1)\,V_{c1}(t_1) + \cdots + S_n(t_1)\,V_{cn}(t_1) \\ \vdots &= \quad \vdots \quad + \cdots + \quad \vdots \\ u_u(t_j) &= S_1(t_j)\,V_{c1}(t_j) + \cdots + S_n(t_j)\,V_{cn}(t_j) \end{aligned} \tag{4}$$

$$\begin{aligned} u_l(t_0) &= S_{n+1}(t_0)\,V_{c(n+1)}(t_0) + \cdots + S_{2n}(t_0)\,V_{c2n}(t_0) \\ u_l(t_1) &= S_{n+1}(t_1)\,V_{c(n+1)}(t_1) + \cdots + S_{2n}(t_1)\,V_{c2n}(t_1) \\ \vdots &= \quad \vdots \quad + \cdots + \quad \vdots \\ u_l(t_j) &= S_{n+1}(t_j)\,V_{c(n+1)}(t_j) + \cdots + S_{2n}(t_j)\,V_{c2n}(t_j) \end{aligned} \tag{5}$$

where the sampling time of the data being processed is assumed to be constant for the whole measurement, in which: $t_1 - t_0 = t_2 - t_1 = \cdots = t_j - t_{j-1} = \Delta t$ (sampling time). Conduction losses and semiconductor voltage drop are neglected in (4) and (5). Therefore, it is assumed that $S_x(t_i) = PWM_x(t_i)$. This assumption has already been proven to be sufficient for the MMC for different voltage estimation techniques [12-14]. As a result, the switching state signals ($PWM_x(t_i)$) can be taken directly from the DSP without the need for extra sensors. Therefore, (4) and (5) can be rewritten in a matrix form as follows:

$$u_u(t_i) = S_x^T(t_i)V_{cx}(t_i) \tag{6}$$
$$u_l(t_i) = S_x^T(t_i)V_{cx}(t_i) \tag{7}$$

Note that, in equation (6) $x = 1, 2, \ldots n$ and in equation (7) $x = (n+1), (n+2), \ldots 2n$.

B. Proposed Kalman Filter Voltage Estimation Scheme.

The KF is a sequential mathematic-based estimator [20] which is widely used in power electronics applications to estimate state and system parameters in differential equations or state-space model representations. The KF has the ability to remove the effect of measurement noise which may be caused by sensors [5, 21, 22]. It is also guaranteed to cope with white Gaussian processing noise [22]. This makes this algorithm superior to some other recursive algorithms.

Table II shows the generalised sequence for KF implementation when a linear system is implemented. For simplicity, it is assumed that the linear dynamic system can be described as follows:

$$y(t_i) = \emptyset_1(t_i)\theta_1(t_i) + \emptyset_2(t_i)\theta_2(t_i) + \cdots + \emptyset_n(t_i)\theta_n \tag{8}$$

where the aim is to identify the values of $\theta_1(t_i), \theta_2(t_i), \ldots \theta_n(t_i)$, for in which $i = 0,1,2, \ldots j$, $y(t_i)$ is the available measured data, and $\emptyset_1(t_i), \emptyset_2(t_i), \ldots \emptyset_n(t_i)$ are other known variables.

Therefore, (8) can be rewritten as follows:

$$y(t_i) = \Phi_x^T(t_i)\theta_x(t_i) \tag{9}$$

where $\Phi_x^T(t_i) = [\emptyset_1(t_i)\ \emptyset_2(t_i)\ \ldots.\emptyset_n(t_i)]^T$

For real system implementation of (9), some other noise is always incorporated with this mathematical model [22]. Therefore, the unknown parameter $\theta(t_i)$ is incorporated with processing noise $w(t_i)$ with covariance matrix $Q(t_i)$, where $Q(t_i)$ is an N×N diagonal matrix. In addition, when the measurement $y(t_i)$ is taken to identify $\theta(t_i)$, measurement noise $v(t_i)$ should also be considered and added to the model. This measurement noise has a variance of $r_{(t_i)}$ where $r(t_i)$ is a positive real number $r(t_i) > 0$ [21]. Therefore, considering such noise with the parameter $\theta(t_i)$ and equation (9) gives the following updated model [21]:

$$\theta(t_i) = \theta(t_{i-1}) + w(t_i) \tag{10}$$
$$y(t_i) = \Phi_x^T(t_i)\theta_x(t_i) + v(t_i) \tag{11}$$

The estimation of $\theta(t_i)$ is performed as demonstrated in the implementation sequence in Table II [5, 21, 22].

Due to the similarity between the linear dynamic model described in (9) and the voltage MMC model described earlier in (6) and (7), a new updated model can be formulated for the MMC. The only difference is to substitute $y(t_i), \Phi_x^T(t_i)$ and $\theta_x(t_i)$ in (9) by total SM arm voltages $u_u(t_i)$ or $u_l(t_i)$, switching states $S_x(t_i)$ and SM voltage $V_{cx}(t_i)$. Therefore, incorporating measurement and processing noise into the model described earlier in (6) and (7) gives the following developed model:

$$u_u(t_i) = S_x^T(t_i)V_{cx}(t_i) + v(t_i) \tag{12}$$
$$u_l(t_i) = S_x^T(t_i)\,V_{cx}(t_i) + v(t_i) \tag{13}$$
$$V_{cx}(t_i) = V_{cx}(t_{i-1}) + w(t_i) \tag{14}$$

TABLE II
GENERAL KF SEQUENCE FOR LINEAR REGRESSION DYNAMIC SYSTEM IMPLEMENTATION

Step	Action and related equation
1. Initialisation	Initiate $P(t_0)$, $\hat{\theta}(t_0)$, $Q(t_0)$ and $r_{(t_i)}$
2. Starting up the algorithm with the same sampling time Δt	For $t_i = t_1, t_2 \ldots t_j$, where $\Delta t = t_{2-}t_1 = t_3 - t_2 = \cdots = t_j - t_{j-1}$
3. Calculate the Kalman gain	$K(t_i) = \dfrac{P(t_{i-1})\Phi(t_i)}{\Phi^T(t_i)P(t_{i-1})\Phi(t_i) + r(t_i)}$
4. Calculate the prediction error	$e_y(t_i) = y(t_i) - \hat{y}(t_i)$
5. Update the parameter $\hat{\theta}(t_i)$	$\hat{\theta}(t_i) = \hat{\theta}(t_{i-1}) + K(t_i)e_y(t_i)$
6. Update the covariance matrix $P(t_i)$	$P_{(t_i)} = P_{(t_i-1)} - \left[\dfrac{P(t_{i-1})\Phi(t_i)\Phi^T(t_i)P(t_{i-1})}{r(t_i) + \Phi^T(t_i)P(t_{i-1})\Phi(t_i)} + Q(t_i)\right]$

Because the upper arm implementation is independent of the lower arm, only the upper arm is described here. Therefore, following the general sequence illustrated in Table II, this results in the following implementation.

To start up the proposed KF algorithm, the covariance matrix $P(t_i)$, and estimated voltage $\hat{V}_{cx}(t_i)$ should be initialized with $P(t_0)$ and $\hat{V}_{cx}(t_0)$. As in conventional recursive algorithms, $P(t_0)$ in the KF algorithm is $P(t_0) = \mathrm{GI}$,

This article has been accepted for publication in a future issue of this journal, but has not been fully edited. Content may change prior to final publication. Citation information: DOI 10.1109/TIE.2018.2795519, IEEE Transactions on Industrial Electronics

where G is a large and positive constant number whilst I is an $x \times x$ identity matrix, where x is the number of SMs. An adaptive Kalman gain is then calculated as follows:

$$K(t_i) = \frac{P(t_{i-1})\, S_x(t_i)}{S_x^T(t_i) P(t_{i-1})\, S_x(t_i) + r(t_i)} \quad (15)$$

Based on the sequence of implementation in Table II, the error of the upper arm is calculated as follows:

$$e_u(t_i) = u_u(t_i) - \hat{u}_u(t_i) \quad (16)$$

As the first sampling time is processed, $P_{(t_{i-1})} = P_{(t_0)}$, and the variance coefficient $r_{(t_i)}$ in this implementation of the KF is defined as a constant number for the whole sampling time, therefore it is assumed that: $r_{(t_1)=} r_{(t_2)=} \dots r_{(t_j)}$. The SM voltage estimation values for the upper arm are then updated with the error calculated using (16) and the Kalman gain derived from (15) and the previously estimated values $\hat{V}_{cx}(t_{i-1})$. Therefore, to estimate these voltages in one prediction step ahead, the upper SM voltage estimated values can be identified as follows:

$$\hat{V}_{cx}(t_i) = \hat{V}_{cx}(t_{i-1}) + K(t_i) e_u(t_i) \quad (17)$$

To further enhance the algorithm, the new covariance matrix is then updated recursively with the values $K_{(t_i)}$ and $Q(t_i)$ as shown in Table II. Therefore, a new prediction step ahead of $P_{(t_{i-1})}$ can be calculated as follows:

$$P_{(t_i)} = P_{(t_i-1)} - \left[\frac{P(t_{i-1})\, S_x(t_i) S_x^T(t_i) P(t_{i-1})}{r(t_i) + S_x^T(t_i) P(t_{i-1})\, S_x(t_i)} + Q(t_i)\right] \quad (18)$$

The proposed upper arm estimation scheme with its associated voltage-balancing control used is shown in Fig.2. The voltage-balancing algorithm used here is similar to the algorithm presented in [23]. It should be noted that the voltage-balancing used in this paper is not linked to the proposed estimation method, which means it is completely independent of the voltage-balancing method used. Therefore, any other voltage control methods can be used with this proposed estimation scheme. In comparison with the algorithm presented in [23], the voltage-balancing of the SM capacitors used here depends on the estimated voltages ($\hat{V}_{c1} \sim \hat{V}_{cn}$) rather than the actual voltages. These voltages $\hat{V}_{c1} \sim \hat{V}_{cn}$, are sorted in descending order to charge and discharge the capacitors depend on upper arm current direction. Once the upper current is positive, the capacitors with the lowest voltage will be charged. On the other hand, when the upper current is negative, the capacitors with the highest voltage will be discharged. The algorithm also defines how many capacitors should be involved in this process. In other words, for each output voltage level, there is a required number (β) of capacitors that need to be charged or discharged. A phase disposition PWM (PD-PWM) is used in the simulation and experimental analyses. A unit delay (Z^{-1}) is applied to the switching patterns ($PWM_1, PWM_2, \dots PWM_n$) obtained in order to switch $S_1, S_2, \dots S_n$ at the appropriate time (see Fig. 2).

For ease of demonstration, assume that the PD-PWM is used for a 4-level MMC only as shown in Fig. 3 and therefore, the number of SMs required for each level can be determined as follows:

- For level one in Fig. 3, the number of the involved SMs for the upper arm, which is determined by switching S_1, S_2 & S_3, is 3. In the same instant, the number required for the lower arm is 0. The total should be always 3 for the whole period of this level (i.e. β_{upper} + β_{lower}=3).
- For level two, the number of the involved SMs for the upper arm, which is determined by switching S_1, S_2 & S_3, is 2 (β_{upper}= 2). In the same instantaneous time, the lower number required for the arm is 1 (β_{lower}=1).
- Similarly, for level three, the number of the SMs involved for the upper arm is 1 and 2 for the lower arm.
- For level four, the number of the involved SMs for the upper arm which is determined by switching S_1, S_2 & S_3, is 0. In the same time, the number required for the lower arm for β_{lower} is 3.

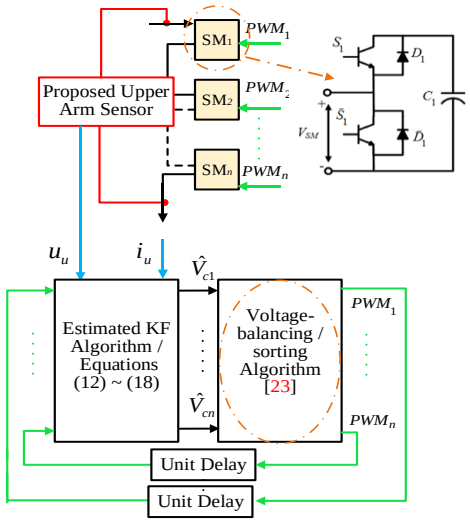

Fig. 2. Upper arm proposed estimation scheme and associated voltage-balancing control for N-level.

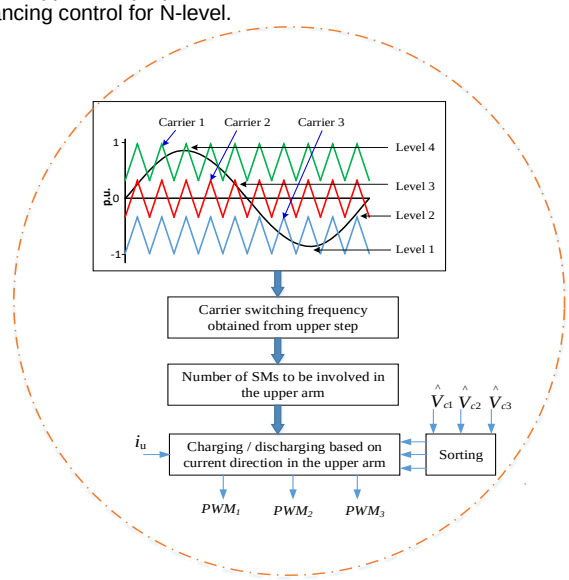

Fig. 3. Voltage-balancing / sorting algorithm for upper arm with 4-level MMC.

This article has been accepted for publication in a future issue of this journal, but has not been fully edited. Content may change prior to final publication. Citation information: DOI 10.1109/TIE.2018.2795519, IEEE Transactions on Industrial Electronics

IV. Simulation Analyses

A single-phase 9-level MMC is simulated using the MATLAB package with the aim of validating the proposed estimation scheme. Sixteen SMs are used for the leg, while one voltage sensor instead of eight per arm is used. The converter, the DC voltage source and the load parameters are tabulated in Table IV. The validation of the proposed method is confirmed below according to the results of different simulations.

A. Steady-State Operation Performance

In this part of the simulation study, a comparison of the proposed estimation scheme and a sensor-based scheme is conducted with a constant R-L load. Fig. 4 shows the performance of the converter waveforms where voltage sensors are used for each SM (sensor-based method). In contrast, Fig. 5 illustrates the performance of the proposed estimation scheme under the same load conditions. In comparing the two methods, only small deviations in the upper arm SM voltages can be observed (see Fig. 5 (a)). However, this error does not have any noticeable effect on neither the output voltage waveform nor the output current waveform. It should be noted that, with the proposed method, only two voltage sensors are used rather than sixteen when the sensor-based method is used.

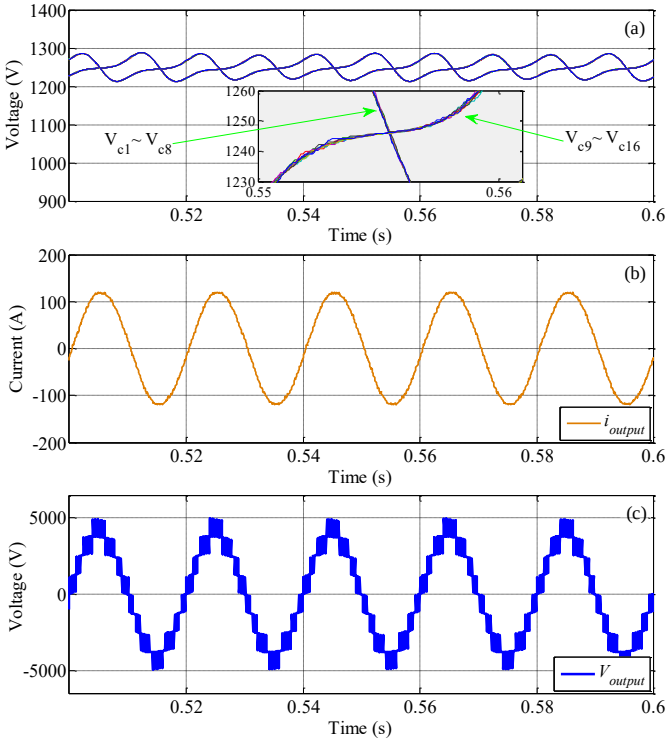

Fig. 4. Steady-state simulation results for the 9-level MMC with the sensor-based method. (a) Upper capacitor voltages V_{c1}~ V_{c8}. (b) Output current. (c) Output voltage.

B. Effect of Parameter Variation

In comparison with the observer-based methods which were proposed in [12, 13], the proposed method is completely independent of variations in arm inductance. This is because the arm inductance is not included in the estimation algorithm design. However, further investigation in terms of capacitance uncertainty is required.

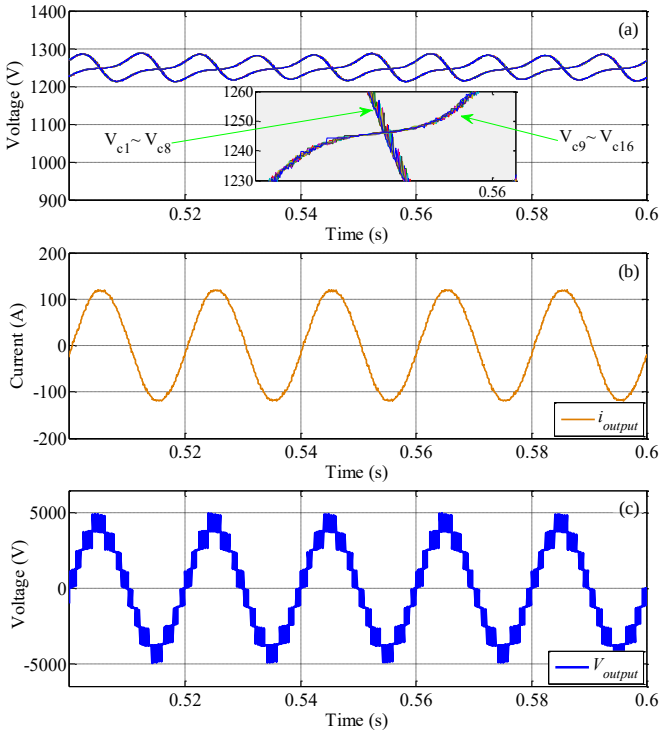

Fig. 5. Steady-state simulation results for the 9-level MMC with the proposed KF estimation scheme. (a) Upper capacitor voltages V_{c1}~ V_{c8}. (b) Output current. (c) Output voltage.

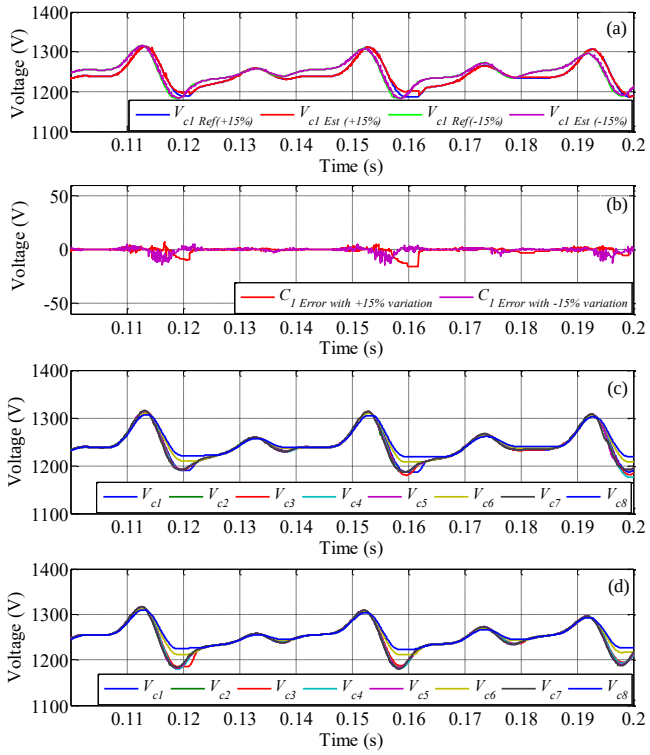

Fig. 6. Results of the upper arm voltages with deviations for all arm capacitors. (a) Reference and estimated voltage across C_1 with ±15% variations. (b) Errors between the reference and estimated voltage when C_1 variations are ±15%. (c) Estimated voltages for all arm capacitors (C_1~C_8) when the deviation is +15%. (d) Estimated voltages for all arm capacitors (C_1~C_8) when the deviation is -15%.

Extensive simulation tests have been carried out to validate the robustness of the proposed estimation method against

This article has been accepted for publication in a future issue of this journal, but has not been fully edited. Content may change prior to final publication. Citation information: DOI 10.1109/TIE.2018.2795519, IEEE Transactions on Industrial Electronics

capacitance variation. Here, C_1 is chosen as an example with different capacitance of deviations: ±15% and ±30%. For each case, random capacitances are chosen for the other SM arm capacitances (C_2~C_8). For example, as shown in Fig. 6 when C_1 has deviations of ±15% from its nominal capacitance (case I), C_2~C_8 are also given random deviations of -20%, +10%, +5%, -15%, +40%, -30%, and +60%.

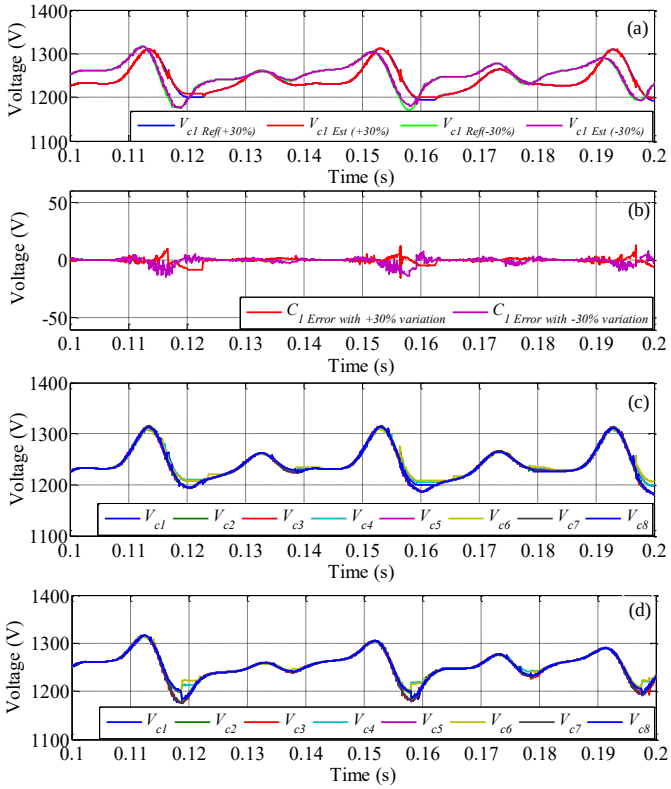

Fig. 7. Results of the upper arm voltages with deviations for all arm capacitors. (a) Reference and estimated voltage across C_1 with ±30% variations. (b) Errors between the reference and estimated voltage when C_1 variations are ±30%. (c) Estimated voltages for all arm capacitors (C_1~C_8) when the deviation is +30%. (d) Estimated voltages for all arm capacitors (C_1~C_8) when the deviation is -30%.

For case I, Fig. 6(a) shows the reference and estimated voltage for C_1 where ±15% variation is considered, and Fig. 6(b) illustrates the error for ±15% variation. It can be observed that the maximum error for both (±15%) is only around 1.3%. Figs 6(c) and 6(d) show the effect of these variations on the other arm capacitors. For case II, C_1 is given as ±30% variations of its nominal capacitance while the other capacitors are given different random capacitances as illustrated in Table III. The error when the variation in C_1 is given as -30% is almost 0.8%; however, with +30% variation the maximum error can be observed to be around 1.1%.

TABLE III
Capacitance Variations in (C_1~C_8)

Capacitor	Case I C1 = ±15% of its nominal	Case II C1 = ±30% of its nominal
C2	-20% =1600μF	+5% =2100μF
C3	+10% =2200μF	-15% =1700μF
C4	+5% =2100μF	+40% =2800μF
C5	-15% =1700μF	-30% =1400μF
C6	+40% =2800μF	+60% =3200μF
C7	-30% =1400μF	-20% =1600μF
C8	+60% =3200μF	+10% =2200μF

C. Effect of Load Change on Estimator Performance

To further validate the proposed estimation scheme, a dynamic test is also carried out with ±100% step change in the load conditions applied to the converter as shown in Fig. 8. At 0.3s the R-L load is increased first by +100% and then at 0.4s

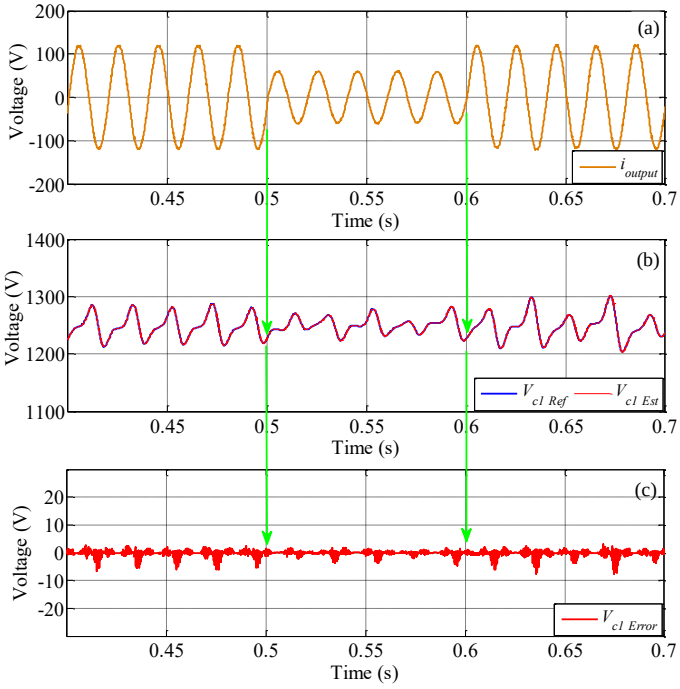

Fig. 8. Effect of step load change on the 9-level MMC. (a) Output current. (b) Voltages across C_1. (c) Voltage estimation Error.

it is forced back to the original value. The effect of these changes on estimated V_{c1} is shown in Fig. 8(b). The estimation error does not exceed 0.6% in both cases as can be seen in Fig. 8(c).

D. Effect of Low Carrier and Effective Switching Frequency on Estimator Performance.

Owing to the ability of the MMC to work at different carrier frequency when different voltage-balancing control methods are used, the proposed estimation method is further investigated, as shown in Fig. 9. The effect of different low carrier frequencies is shown respectively (f_c =1500, 250 and 45 Hz) for all eight SMs. Column (a) in the figure for example, represents the voltage error for SM1 to SM8 respectively when f_c = 1500 Hz. For all carrier frequencies used, the error of the estimation voltage across C_1 does not exceed 1%. These results confirm the ability of the proposed method to work at low carrier frequency. Another test has been carried out in Fig. 10 to investigate the effect of using voltage-balancing method with low effective switching reduction on the proposed estimation scheme. Similar to the method introduced in [24] has been implemented for this test.

E. DC Fault and Start-up Performance

To further validate the proposed estimation scheme, a fault in the DC source is applied to the MMC. In this case study, a sudden drop of 50% in the DC voltage is considered. The corresponding changes in the output waveforms of the converter as well as the performance of the voltage estimation across C_1 are shown in Fig. 11 (a), (b) and (c) respectively.

This article has been accepted for publication in a future issue of this journal, but has not been fully edited. Content may change prior to final publication. Citation information: DOI 10.1109/TIE.2018.2795519, IEEE Transactions on Industrial Electronics

The start-up estimation performance of V_{C1} is shown in Fig. 12. For the reference voltage, the capacitor is assumed to be pre-charged at its reference voltage (i.e. $V_{C1}(t_0)$ = 1250 V). As can be seen from Fig. 12 the proposed KF estimation scheme successfully traced the reference voltage within a very short time.

V. Experimental Analyses

A single-phase 4-level MMC scaled down laboratory prototype is developed to validate the proposed estimation scheme. Fig. 13(a) shows the block diagram of the complete experimental platform, whilst the real set-up of the experimental test bench is shown in Fig. 13(b). The converter consists of six SMs. The switching devices used are IRF530N power MOSFET, whilst the SM capacitors are the VISHAY 56 1000µF with a rated voltage of 63V. According to the manufacturer the capacitor variations are ± 20%. Table IV shows more details about the system including the R-L load values. A TMS320F28335 controller (Texas Instruments) is used to control the converter. The proposed KF estimation algorithm and the voltage-balancing algorithm are uploaded to the controller with the help of Code Composer Studio (CCS5.5) development tools.

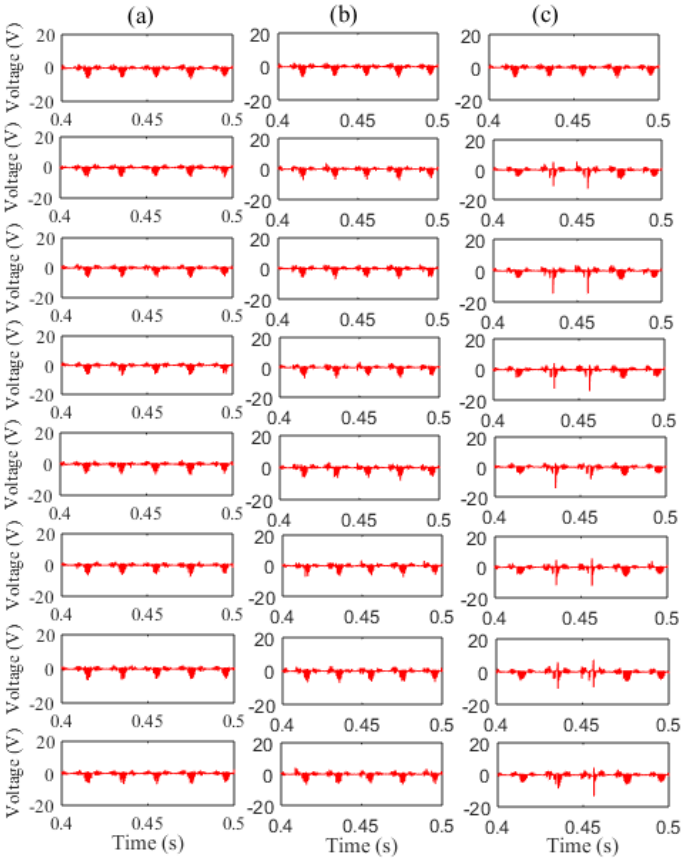

Fig. 9. Performance of the proposed estimation scheme with low carrier frequencies for all eight SMs. (a) Voltage error across $C_1 \sim C_8$ when f_c=1.5 kHz was used. (b) Voltage error across $C_1 \sim C_8$ when f_c = 750 Hz was used. (c) Voltage error across $C_1 \sim C_8$ when f_c = 45 Hz was used.

This is accomplished using the Embedded Coder Support Package in MATLAB/Simulink to generate the required C code for all associated blocks in the MATLAB/Simulink models. The converter is operated at 2.5 kHz switching frequency with a dead-time of 3μs.

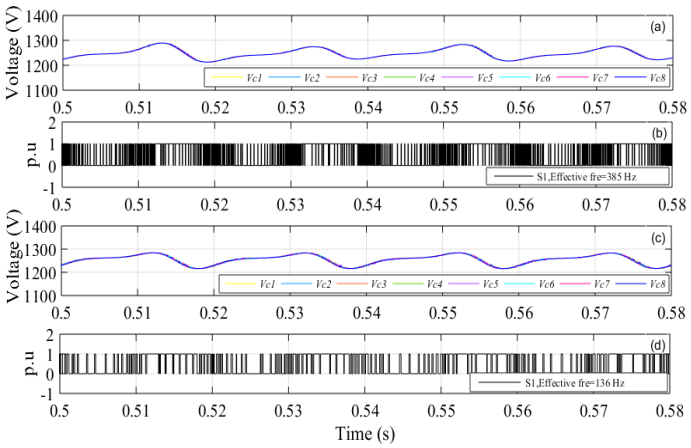

Fig. 10. The effect of effective switching frequency on the proposed estimation method. (a) Estimated voltages for $V_{c1} \sim V_{c8}$ based on [23]. (b) Effective switching frequency for S1. (c) Estimated voltages for $V_{c1} \sim V_{c8}$ based on [24]. (d) Effective switching frequency for S1.

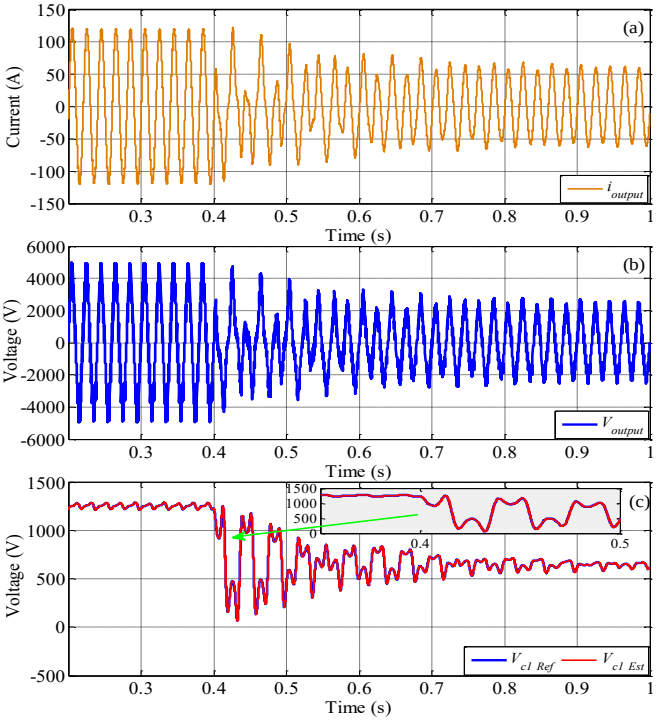

Fig. 11. Performance of the proposed method during DC fault. (a) Output current response. (b) Output voltage response. (c) The effect of the DC fault on the estimated V_{c1}.

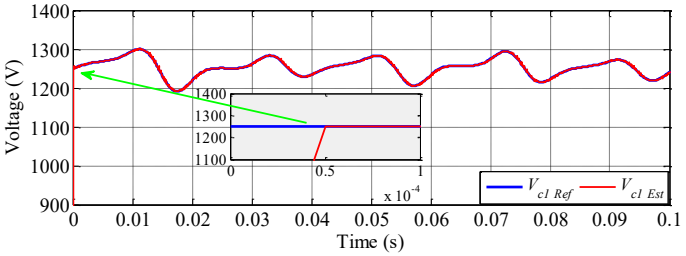

Fig. 12. Performance of the proposed estimation scheme during start-up transient condition.

This article has been accepted for publication in a future issue of this journal, but has not been fully edited. Content may change prior to final publication. Citation information: DOI 10.1109/TIE.2018.2795519, IEEE Transactions on Industrial Electronics

To evaluate the performance of the proposed estimation scheme, extensive testes at different operating conditions are carried out, including investigation of steady-state and dynamic analyses.

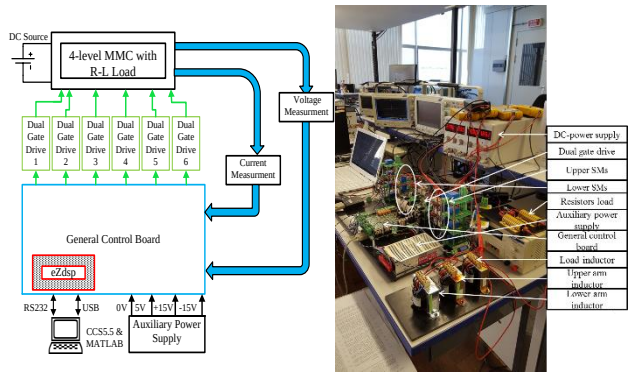

(a) (b)

Fig. 13. Experimental set-up. (a). Block diagram. (b). The experimental test bench.

TABLE IV
SIMULATION AND EXPERIMENTAL PARAMETERS

Parameter	Simulation	Experimental
SM capacitor (**C**)	3800 µF	1000 µF
Modulation index ($\mathbf{m_i}$)	0.80	0.9
DC-link voltage ($\mathbf{V_{dc}}$)	10 kV	60V
Output frequency (**f**)	50 Hz	50 Hz
Carrier frequency ($\mathbf{f_c}$)	2.5 kHz	2.5 kHz
Number of SM per leg (**N**)	16	6
Load resistor (**R**)	33& 66 Ω	33& 68 Ω
Arm inductor ($\mathbf{L_S}$)	3.6 mH	1 mH
Load inductor (**L**)	15 mH	4 mH
Power (S)	240 kVA	24.3 VA
Sampling frequency ($\mathbf{f_{sampling}}$)	20 kHz	20 kHz

A. Steady-State Operation Performance

A comparison has been made between the proposed estimation scheme and the sensor-based method to verify the simulation results. A constant R-L load is applied to the converter, and its output waveforms are illustrated in Fig. 13 based on the sensor-based method. The three upper capacitor voltages are shown in Fig. 14 (a), whilst the output load current and voltage waveforms are shown in Fig. 14(b) and (c). Comparison with the proposed estimation scheme, Fig. 15 (b) and (c) shows no differences in terms of the output converter waveforms for current and voltage. However, similar to the results achieved earlier in the simulation analysis, the three capacitor voltages shown in Fig. 15 (a) exhibit slight deviations in comparison with those in Fig. 14 (a). However, as described above, there is no noticeable impact on the output waveforms of the converter, which validates the simulation results. Zoomed-in output wave forms of Fig. 14(b), (c) and Fig. 15 (b), (c) are illustrated in Fig. 16 (a) and (b) respectively. In addition, Fig. 17 compares between measured and estimated voltage across C_1, C_2 and C_3. Samples of the measured voltages for the upper and lower arms are illustrated in Fig. 18.

B. Effect of Load Change on Performance

Further validation for dynamic change operation is illustrated in Fig. 19. In this study, step changes in the load resistance (R) are considered, where the value of R is altered between 33 Ω and 68 Ω first, and then between 68 Ω and 33 Ω. For both cases, as can be seen in Fig. 19, the capacitor voltages still track the reference voltage ($\frac{\mathrm{Vdc}}{\mathrm{n}}$), which confirms the simulation results.

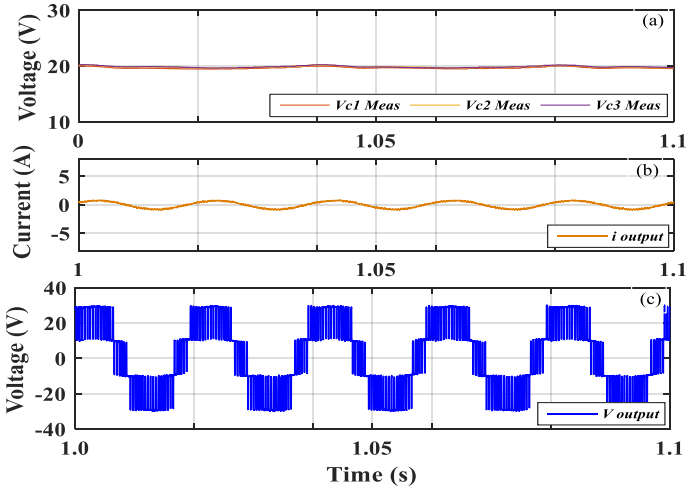

Fig. 14. Experimental results of the sensor-based method at constant R-L load. (a) Upper SM voltage capacitors. (b) Output current and voltage waveforms.

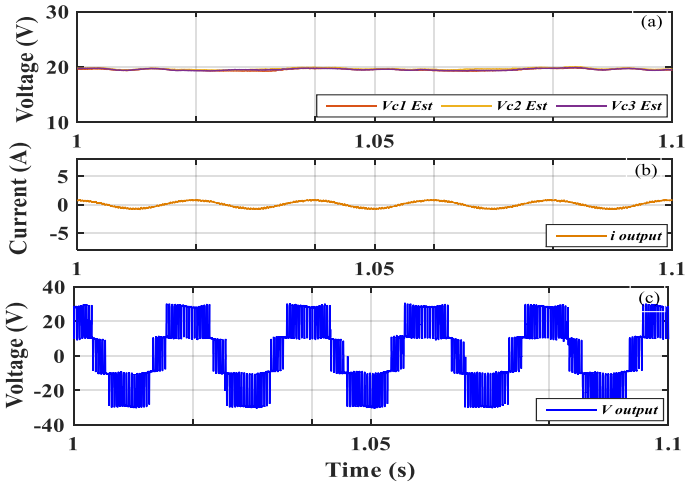

Fig. 15. Experimental results of the proposed estimation scheme at constant R-L load. (a) Upper SM voltage capacitors. (b) Output current and voltage waveforms.

C. Effect of DC Fault on the Estimation Performance

To further confirm the robustness of the proposed scheme in terms of more dynamic changes, another case has been investigated. A DC voltage fault is applied to the MMC by applying a sudden extreme change in the DC voltage applied to the converter. The DC input voltage of the converter has been decreased by around 90%. Although this is an extreme change in the DC voltage, the proposed scheme successfully tracks this change as shown in Fig. 20, where the estimated voltage $\hat{V}_{c1}$ matches its reference voltage ($\frac{\mathrm{Vdc}}{\mathrm{n}}$).

D. Extreme Increase in the DC Source

An extra change is also examined in Fig. 21, where a sudden increase in the DC voltage is applied in this case. In this

This article has been accepted for publication in a future issue of this journal, but has not been fully edited. Content may change prior to final publication. Citation information: DOI 10.1109/TIE.2018.2795519, IEEE Transactions on Industrial Electronics

investigation, a sudden increase of approximately 90% in the DC voltage is applied to the system. It can be observed from Fig. 21 that the voltage across C_1 rapidly and successfully reacts to this change.

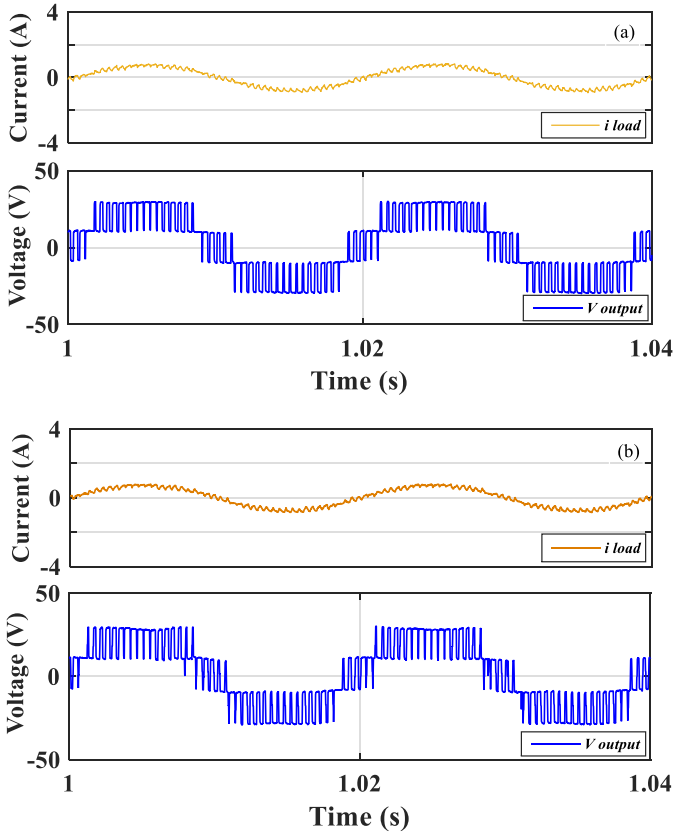

Fig. 16. Zoomed-in of output voltage and current of the sensor-based method and proposed estimation scheme. (a) Output voltage and current of sensor-based scheme. (b) Output voltage and current of the proposed estimation scheme.

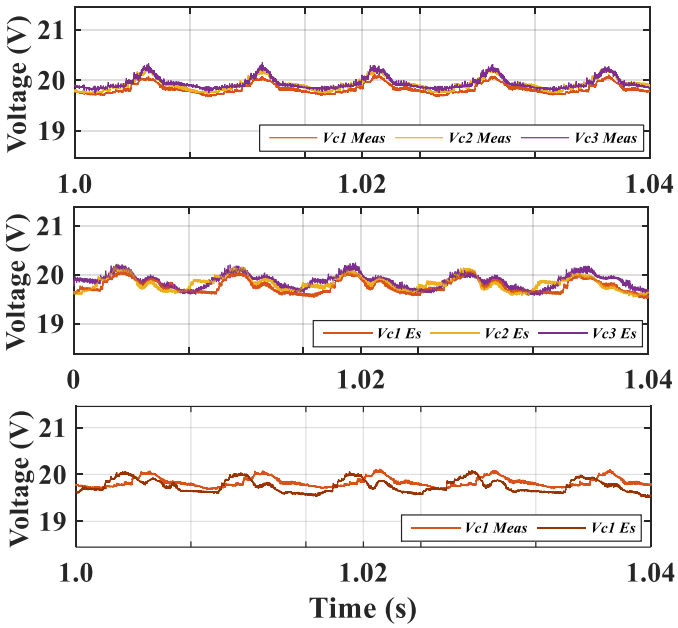

Fig. 17. Experimental results of the voltages across C_1, C_2 and C_3 when the sensor-based method and proposed estimation scheme are used. (a) Zoomed-in V_{c1}, V_{c2} and V_{c3}. (b) Zoomed-in $\hat{V}_{c1}, \hat{V}_{c2}$ and $\hat{V}_{c3}$

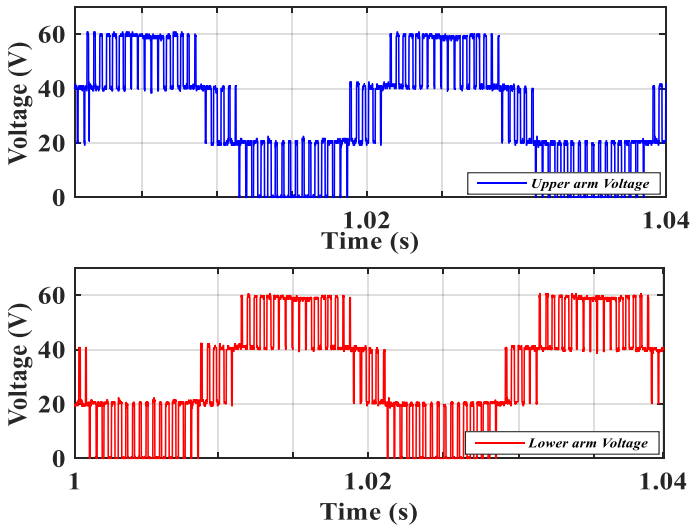

Fig. 18. Upper and lower arm voltages.

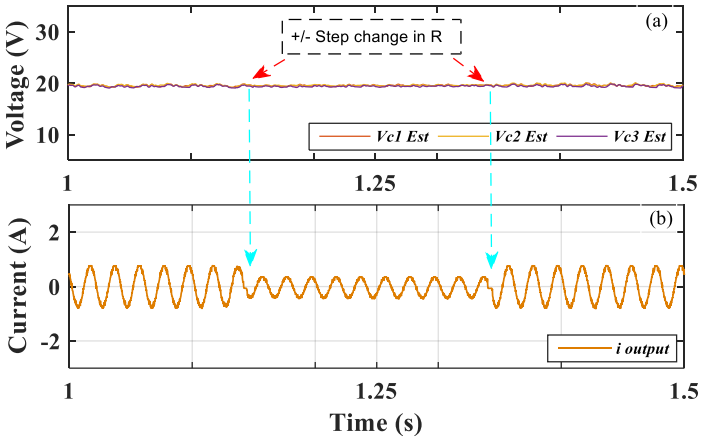

Fig. 19. Step load change analysis of the load resistance (R) in the proposed method.

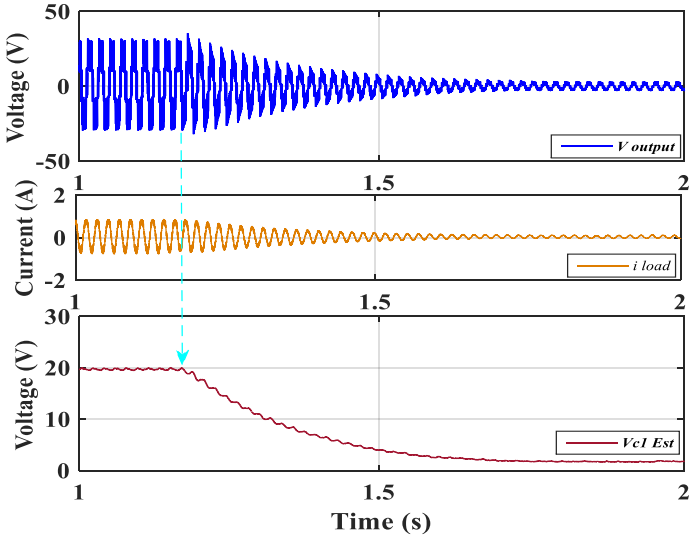

Fig. 20. Fault in the DC voltage and corresponding changes in converter waveforms.

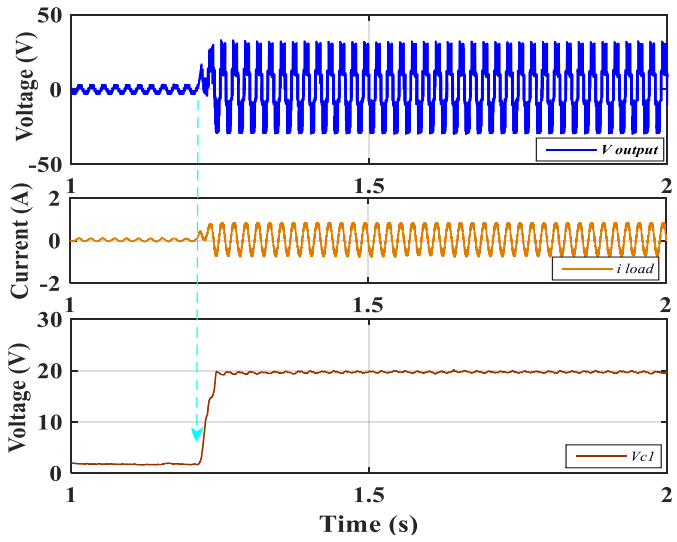

Fig. 21. Extreme increase in DC voltage and corresponding changes in converter waveforms.

VI. Conclusion

In this paper, a new voltage estimation scheme for the MMC is proposed in which a new employment of the KF algorithm is developed for the converter. Comprehensive studies of a one-leg MMC have been conducted to demonstrate the effectiveness of the proposed scheme in simulation and experimental environment analyses. Extensive steady-state and dynamic analyses have been performed. The results show that the proposed estimation scheme succeeded in providing accurate voltage estimation results, and therefore the voltage-balancing of the MMC is achieved with only one voltage sensor per arm. Using this proposed scheme, any conventional voltage-balancing technique can be easily incorporated. This development facilitates an important reduction in the number of voltage sensors required. Consequently, this improvement will reduce the total cost of the converter and reduce its complexity. The most promising application of the proposed scheme is to contribute a strategy to identify faults. Finally, the proposed method can also be applied to CHCs and FCCs.

References

[1] A. Lesnicar, and R. Marquardt, "An Innovative Modular Multilevel Converter Topology Suitable for a Wide Power Range." p. 6 pp. Vol.3.

[2] F. Deng, Y. Tian, R. Zhu, and Z. Chen, "Fault-Tolerant Approach for Modular Multilevel Converters Under Submodule Faults," *IEEE Transactions on Industrial Electronics,* vol. 63, no. 11, pp. 7253-7263, 2016.

[3] H. Yang, and M. Saeedifard, "A Capacitor Voltage Balancing Strategy With Minimized AC Circulating Current for the DC–DC Modular Multilevel Converter," *IEEE Transactions on Industrial Electronics,* vol. 64, no. 2, pp. 956-965, 2017.

[4] K. Shen, D. Zhao, J. Mei, L. M. Tolbert, J. Wang, M. Ban, Y. Ji, and X. Cai, "Elimination of Harmonics in a Modular Multilevel Converter Using Particle Swarm Optimization-Based Staircase Modulation Strategy," *IEEE Transactions on Industrial Electronics,* vol. 61, no. 10, pp. 5311-5322, 2014.

[5] F. Deng, Z. Chen, M. R. Khan, and R. Zhu, "Fault Detection and Localization Method for Modular Multilevel Converters," *IEEE Transactions on Power Electronics,* vol. 30, no. 5, pp. 2721-2732, 2015.

[6] M. Guan, and Z. Xu, "Modeling and Control of a Modular Multilevel Converter-Based HVDC System Under Unbalanced Grid Conditions," *IEEE Transactions on Power Electronics,* vol. 27, no. 12, pp. 4858-4867, 2012.

[7] G. Konstantinou, J. Pou, S. Ceballos, R. Picas, J. Zaragoza, and V. G. Agelidis, "Control of Circulating Currents in Modular Multilevel Converters Through Redundant Voltage Levels," *IEEE Transactions on Power Electronics,* vol. 31, no. 11, pp. 7761-7769, 2016.

[8] A. Dekka, B. Wu, N. R. Zargari, and R. L. Fuentes, "A Space-Vector PWM-Based Voltage-Balancing Approach With Reduced Current Sensors for Modular Multilevel Converter," *IEEE Transactions on Industrial Electronics,* vol. 63, no. 5, pp. 2734-2745, 2016.

[9] F. Deng, and Z. Chen, "Voltage-Balancing Method for Modular Multilevel Converters Switched at Grid Frequency," *IEEE Transactions on Industrial Electronics,* vol. 62, no. 5, pp. 2835-2847, 2015.

[10] F. Deng, and Z. Chen, "A Control Method for Voltage Balancing in Modular Multilevel Converters," *IEEE Transactions on Power Electronics,* vol. 29, no. 1, pp. 66-76, 2014.

[11] K. Ilves, A. Antonopoulos, S. Norrga, and H. P. Nee, "A New Modulation Method for the Modular Multilevel Converter Allowing Fundamental Switching Frequency," *IEEE Transactions on Power Electronics,* vol. 27, no. 8, pp. 3482-3494, 2012.

[12] S. Shao, P. W. Wheeler, J. C. Clare, and A. J. Watson, "Fault Detection for Modular Multilevel Converters Based on Sliding Mode Observer," *IEEE Transactions on Power Electronics,* vol. 28, no. 11, pp. 4867-4872, 2013.

[13] H. Nademi, A. Das, and L. E. Norum, "Modular Multilevel Converter With an Adaptive Observer of Capacitor Voltages," *IEEE Transactions on Power Electronics,* vol. 30, no. 1, pp. 235-248, 2015.

[14] R. Picas, J. Zaragoza, J. Pou, S. Ceballos, and J. Balcells, "New Measuring Technique for Reducing the Number of Voltage Sensors in Modular Multilevel Converters," *IEEE Transactions on Power Electronics,* vol. 31, no. 1, pp. 177-187, 2016.

[15] R. Picas, J. Zaragoza, J. Pou, and S. Ceballos, "Reliable Modular Multilevel Converter Fault Detection With Redundant Voltage Sensor," *IEEE Transactions on Power Electronics,* vol. 32, no. 1, pp. 39-51, 2017.

[16] S. Debnath, J. Qin, B. Bahrani, M. Saeedifard, and P. Barbosa, "Operation, Control, and Applications of the Modular Multilevel Converter: A Review," *IEEE Transactions on Power Electronics,* vol. 30, no. 1, pp. 37-53, 2015.

[17] H. Akagi, "Classification, Terminology, and Application of the Modular Multilevel Cascade Converter (MMCC)," *IEEE Transactions on Power Electronics,* vol. 26, no. 11, pp. 3119-3130, 2011.

[18] A. Dekka, B. Wu, N. R. Zargari, and R. L. Fuentes, "Dynamic Voltage Balancing Algorithm for Modular Multilevel Converter: A Unique Solution," *IEEE Transactions on Power Electronics,* vol. 31, no. 2, pp. 952-963, 2016.

[19] P. M. Meshram, and V. B. Borghate, "A Simplified Nearest Level Control (NLC) Voltage Balancing Method for Modular Multilevel Converter (MMC)," *IEEE Transactions on Power Electronics,* vol. 30, no. 1, pp. 450-462, 2015.

[20] M. A. Eleffendi, and C. M. Johnson, "Application of Kalman Filter to Estimate Junction Temperature in IGBT Power Modules," *IEEE Transactions on Power Electronics,* vol. 31, no. 2, pp. 1576-1587, 2016.

[21] L. Cao, and H. M. Schwartz, "Analysis of the Kalman filter based estimation algorithm: an orthogonal decomposition approach," *Automatica,* vol. 40, no. 1, pp. 5-19, 1//, 2004.

[22] R. Antonello, K. Ito, and R. Oboe, "Acceleration Measurement Drift Rejection in Motion Control Systems by Augmented-State Kinematic Kalman Filter," *IEEE Transactions on Industrial Electronics,* vol. 63, no. 3, pp. 1953-1961, 2016.

[23] M. Saeedifard, and R. Iravani, "Dynamic Performance of a Modular Multilevel Back-to-Back HVDC System," *IEEE Transactions on Power Delivery,* vol. 25, no. 4, pp. 2903-2912, 2010.

[24] Q. Tu, Z. Xu, and L. Xu, "Reduced Switching-Frequency Modulation and Circulating Current Suppression for Modular Multilevel Converters," *IEEE Transactions on Power Electronics,* vol. 26, no. 3, pp. 2009-2017, 2011.

Osama SH Mohamed Abushafa received the B.Sc. degree in Electrical and Electroni Department from Sirt University, Albregah, Libya in 2001, M.Sc. and the Ph.D. degrees from Newcastle University, Newcastle upon Tyne, U.K., in 2010, and 2017. From 2010 to 2012, he was an Assistant Lecturer with the Department of Electrical and Electronic Department, Zawia University. In 2013, he joined the Electrical Power Research Group, Newcastle University, as a PhD researcher in Power Electronics. Since November 2017, Dr Osama has joined Turbo Power Systems LTD company. Dr. Osama has been recently a Regular Reviewer for IEEE journals

Mohamed S. A. Dahidah (M'02–SM'10) received the Ph.D. degree in electrical engineering from Multimedia University, Malaysia, in 2008. In November 2007, he was appointed an Assistant Professor in the Department of Electrical and Electronic Engineering, The University of Nottingham, Malaysia Campus. He is currently with the School of Engineering, Newcastle University, Newcastle Upon Tyne, U.K. He has authored or co-authored a number of refereed journal and conference papers. His research interests include modular multilevel converters, SHE-PWM modulation technique for power electronics converters, battery charger for EVs, solid state transformers and renewable energy integration.
Dr. Dahidah is the Deputy Editor-in-Chief for IET Power Electronics and has been a Regular Reviewer for both IEEE and IET journals.

Shady Gadoue received the B.Sc. and M.Sc. degrees from Alexandria University, Alexandria, Egypt, in 2000 and 2003, respectively, and the Ph.D. degree from Newcastle University, Newcastle upon Tyne, U.K., in 2009, all in Electrical Engineering. From 2009 to 2011, he was an Assistant Professor with the Department of Electrical Power Engineering, Alexandria University. In 2011, he joined the Electrical Power Research Group, Newcastle University, as a Lecturer in Control Systems. Since March 2016, Dr Gadoue has been a visiting member of academic staff with the Control and Power Research Group at Imperial College London, U.K. In Aug 2017, he joined the School of Engineering and Applied Science, Aston University, Birmingham as a Senior Lecturer. His main research interests include control, state and parameter identification, and optimization algorithms applied to energy conversion and power electronic systems.

David J. Atkinson obtained his BSc in electrical and electronic engineering from Sunderland Polytechnic, England, in 1978 and his PhD from Newcastle University, England, in 1991. He is a Senior Lecturer in the Electrical Power Research Group at the School of Electrical and Electronic Engineering, Newcastle University, UK. He joined the university in 1987 after 17 years in industry with NEI Reyrolle Ltd and British Gas Corporation. His research interests are focussed on the control of power electronics systems including electric drives and converters for renewable energy systems. Dr Atkinson is a chartered electrical engineer and a recipient of the Power Premium awarded by the Institution of Electrical Engineers (IEE).

.